The DTU21 Global Mean Sea Surface and First Evaluation

Ole Baltazar Andersen[1], Stine Kildegaard Rose[1], Adili Abulaitijiang[2], Shengjun Zhang[3], Sara Fleury[4]

[1] DTU space, National Space Institute, Elektrovej 327/328, DK-2800 Kongens Lyngby, Denmark.
[2] University of Bonn, Institute of Geodesy and Geoinformation Nussallee 17, D-53115 Bonn, Germany
[3] School of Resources and Civil Engineering, Northeastern University, Shenyang, China
[4] LEGOS, Observatoire Midi-Pyrénées 14, avenue Édouard Belin 31400, Toulouse, France

Correspondence to: Ole B. Andersen oa@space.dtu.dk

Abstract. A new Mean Sea Surface (MSS) called DTU21MSS for referencing sea level anomalies from satellite altimetry is introduced in this paper and a suite of evaluations are performed. One of the reasons for updating the existing Mean Sea Surface is the fact, that during the last 6 years nearly three times as much data have been made available by the space agencies, resulting in more than 15 years of altimetry from Long Repeat Orbits or Geodetic Missions. This includes the two interleaved long repeat cycles of Jason-2 with a systematic cross-track distance as low as 4 km.
A new processing chain with updated filtering and editing has been implemented for DTU21MSS. This way, the DTU21MSS has been computed from 2Hz altimetry in contrast to the former DTU15MSS/DTU18MSS which were computed from 1 Hz altimetry. The new DTU21MSS is computed over the same 20-year averaging time from 1993.01.01 to 2012.12.31 with a well-specified central time of 2003.01.01 and is available from the following site; (https://doi.org/10.11583/DTU.19383221.v1, Andersen, 2022)
Cryosat-2 employs SAR and SARin modes in a large part of the Arctic Ocean due to the presence of sea ice. For SAR and SARin mode data we applied the SAMOSA+ physical retracking to make it compatible with the physical retracker used for conventional Low-Resolution Mode data in other parts of the ocean.

1 Introduction

Satellite altimetry provides highly accurate measurements of the ocean topography along the ground tracks of the satellite (Fu and Cazenave, 2001; Stammer and Cazenave, 2017). For oceanography, the anomalous sea level about a mean reference surface is of primary interest. During the last two decades, Mean Sea Surface (MSS) as a reference surface has been developed with increasing accuracy (Pujol et al., 2017), Yuan et al., 2023).
Mean sea surface models are increasingly used as vertical offshore reference surfaces for offshore operations (e.g., dredging, windfarms, bathymetry surveys)
To develop a MSS it would be optimal if observations were available on all time and spatial scales. The challenge is to derive an MSS given limited sampling in both time and space using satellite

observations. Another challenge is to merge repeated observations along coarse ground tracks with high spatial data from the geodetic mission (GM).
Thanks to new altimeter instruments and processing technology the accuracy of observed Sea Surface Height (SSH) has increased dramatically over the last decade. Sea Level Anomalies (SLA) are referenced to a global MSS. It is consequently important that the MSS is as accurate as possible when investigating smaller mesoscale features (e.g., Dufau et al., 2016).
The paper is structured in the following way. Chapter 2 presents the details of the derivation of the new DTU21MSS with a focus on the improvement in data, retracking, processing and filtering. The chapter is concluded with a subsection on the potential use of SAR altimetry from Sentinel-3A/B for the DTU21MSS. Chapter 3 highlights various comparisons ranging from global comparison to regional evaluations in the Arctic Ocean and for coastal regions illustrating the improvement in the DTU21MSS model.

2. Computation of the DTU21MSS

The DTU21MSS is based on satellite altimetry data from frequently repeating Exact Repeat Missions (ERM) and in-frequently missions with long or drifting repeat – called Geodetic Mission (GM). The MSS is determined from a sophisticated combination of the coarse ERM with the high-density GM data as described in Andersen and Knudsen (2008). In the derivation of the MSS coarse ERM data are used to derive the coarse MSS. Subsequently, the GM data are introduced to derive the fine-scale features in the MSS.
The long wavelength MSS was derived using the highly accurate nearly uninterrupted mean profiles derived using TOPEX/J1/J2. These data were taken from the 1 Hz data from the Radar Altimetry Data Archive (RADS, Scharroo et al., 2013). To extend the MSS into the polar regions outside the 66º parallel and to enhance the spectral resolution the other mean profiles shown in Table 1 from other Exact repeating satellites were fitted to the TOPEX/J1/J2 profiles. The differences were found by computing crossover differences between the ERM datasets. The crossover residuals were expanded into spherical harmonic degrees and order 2 to 4 and this surface was used to correct the ERM datasets. This methodology was similarly applied to derive DTU15MSS and DTU18MSS. Hence as a prior long wavelength model, we used a filtered version of the DTU18 MSS for wavelength greater than 100 km. For reference, the filtered version of DTU18MSS and DTU15MSS are virtually identical inside the 66º parallel.
Before the MSS is computed the averaging period and consequently the center time for the MSS was selected. We used an averaging period from 1993.01.01 to 2012.12.31. Hence the center time for DTU21MSS and previous DTU models will be 2003.01.01.
There has been a significant focus on the accuracy of MSS models (Pujol et al., 2019) in the preparation for the Surface Water and Ocean Topography (SWOT) mission launched recently. We consequently decided to keep the same 20-year averaging period for DTU21MSS to be able to validate the MSS directly with other MSS models. Changing the averaging period by as little as 3 years will change the mean by 1 cm as well as the spatial pattern due to ongoing sea level change (Veng and Andersen, 2019).

Table 1 shows all altimetry used for the computation of the DTU21MSS and its predecessors: DTU15MSS and DTU18MSS. Whereas the DTU15MSS was based on roughly 5 years of GM observations, the DTU21MSS is based on nearly three times as much data or more than 15 years of GM due to the recent focus on prioritizing long repeat orbits.
Satellite observations from the four newer GMs (Cryosat-2, Jason-1, Jason-2 & SARAL) have around 1.5 times higher range precision compared with the old ERS-1 and Geosat GM (Garcia et al., 2014). Consequently, it was decided to retire the older ERS1 and Geosat GM data for the DTU21MSS.

	Satellite	DTU15MSS	DTU18MSS	DTU21MSS
ERM	TP+Jason-1+Jason-2	Jan 1993- Dec 2012	Jan 1993- Dec 2012	Jan 1993-Dec 2012
	ERS2+ENVISAT	May 1996-Oct 2011	May 1996-Oct 2011	May 1996-Oct 2011
	TP & Jason-1 Interleaved	Sep 2002 to Oct 2005 Feb 2009 to Mar 2012	Sep 2002 to Oct 2005 Feb 2009 to Mar 2012	Sep 2002 to Oct 2005 Feb 2009 to Mar 2012
	GFO	Jan 2001 Aug 2008	Jan 2001 Aug 2008	Jan 2001 Aug 2008
GM	ERS1 (2 interleaved cycles of 168 days)	April 1994-May 1995	April 1994-May 1995	Not Used
	Cryosat-2 (368.25 days repeat	Oct 2010-July 2014	Oct 2010-July 2017	Oct 2010- Oct 2019
	Jason1 LRO (1 cycle of 404 days)	April 2012-Jun 2013	April 2012-Jun 2013	April 2012-Jun 2013
	Jason2 LRO (2 cycles of 371 days)	Not used	Not used	Aug 2017-Sept 2019
	Saral AltiKa (drifting phase)	Not used	Not used	July 2016-Dec 2020

Table 1: Satellite altimetry used for the DTU15/18/21MSS models.

The following sections describe the theoretical and practical advances leading up to the release of the DTU21MSS. The next section describes the short wavelength improvement and the subsequent section the improvement to the long wavelength part in the Polar regions.

2.1 Short wavelength MSS from Geodetic Mission altimetry

The short wavelength part of the MSS is derived from the geodetic mission (GM) data. The Sensor Geophysical Data Record (SGDR) products for Jason-1 GM, Jason-2 GM, and SARAL/AltiKa GM are obtained from the Archiving, Validation, and Interpretation of Satellite Oceanographic (AVISO) data service. The L1b-level products for CryoSat-2 LRM are acquired through the data distribution service of the European Space Agency (ESA). All these products include along-track 20 Hz waveforms for all missions except for 40 Hz waveforms for SARAL/AltiKa.
All environmental and geophysical corrections of the altimeter range measurements have been applied to calculating SSH. These corrections include dry and wet tropospheric path delay, ionospheric correction, ocean tide, solid earth tide, pole tide, high-frequency wind effect, and inverted barometer correction. The most recent FES2014 ocean tide model has been used for all missions (Lyard et al., 2021). All corrections are provided on 1-Hz. Hence, these were interpolated into 20 Hz or 40 Hz by using piecewise cubic spline interpolation.
All satellites except for CryoSat-2 operate in the traditional low-resolution mode (LRM) where the along-track resolution is limited to 2-3 km. Cryosat-2 also operates in LRM over most of the oceans. In regions where sea ice is prevailing Cryosat-2 operates in Synthetic Aperture Radar (SAR) mode. In this mode, the returning echoes are processed coherently resulting in a footprint of 290 meters. Over steeply varying terrain and in some coastal regions, the SAR interferometric mode (SARin) is used

where the instrument receives on two antennas are used. A mode mask controls the availability of three Cryosat-2 data types (web1, 2022). The advantage of SAR processing is a near two-time range-precision improvement (Raney, 2011). Due to the burst structures of Cryosat-2, the improvement found is only around 1.5 times the range precision of LRM data. (Raney, 2011; Garcia et al., 2014)
Waveform retracking is an effective strategy to improve the range precision of altimeter echoes (Gommenginger et al., 2001). There are two strategies. Empirical retracker has the advantage of providing a valid and robust estimation of arrival time used to determine the SSH over almost all types of surfaces (e.g., sea ice leads, coastal). The disadvantage is, that empirical retrackers only provide SSH and not rise time used to determine significant wave height and wind speed. Hence it's not possible to determine the sea state bias correction to the SSH observations (Fu and Cazenave, 2001).
Physical retrackers generally apply the Brown model for LRM data (Brown, 1977) or the SAMOSA model for SAR and SAR-in observations (Ray et al., 2015). These retrackers estimate 3 or more parameters and enable corrections and sea state conditions, through the determination of significant wave height and wind speed. Hence these enable the determination of, and subsequent correction for sea state bias correction.

2.1.1 Two-pass retracking for range precision

Over the ocean, the waveforms from all four GM satellite missions are well-modeled and retracked using the Brown-type model. In the first step, the waveforms are fitted by the three-parameter Brown model (arrival time, rise time, and amplitude).
Maus et al. (1998) and Sandwell and Smith (2005) demonstrated the presence of a strong coherence between the estimation errors in the arrival time and rise time parameters resulting in a relatively noisy estimate of arrival time and hence sea surface height. Consequently, Sandwell and Smith (2005) suggested the use of a second step where the rise time parameter is smoothed. In the derivation of the DTU21MSS, we applied the same two-step retracking and fixed the along-track smoothing at 40 km before retracking the waveforms again using a two-parameter waveform model (fitting only arrival time and amplitude).
For all four recent GM missions (Jason-1, Jason-2, SARAL/AltiKa, and CryoSat-2/LRM) this approach has been proved effective (Garcia et al., 2014; Zhang and Sandwell, 2017). Figure 1 illustrates the gain in range precision using the two-pass retracking. The improvement for all four LRM datasets is dependent on the SWH but is on average of the order of 1.5 similarly to other studies (Sandwell et al., 2014; Zhang et al., 2019).

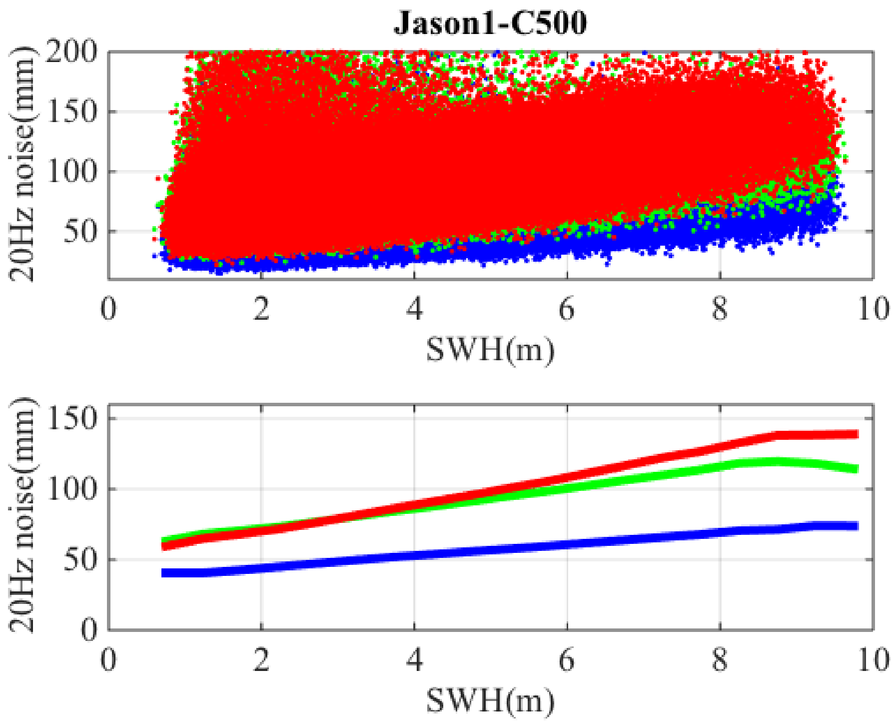

Figure 1: The standard deviation of retracked height with respect to DTU15MSS for cycle 500 (corresponds to the first 11 days of the Jason-1 GM). The upper figure illustrates the statistics for individual points. The lower figure illustrates the median averaged over 0.5 meters SWH intervals. Red: height from sensor geophysical data record; Green: height from the first step of two-pass retracking; Blue: height from the second step of the two-pass retracking). Modified from Andersen et al., (2021)

Whereas two-pass retracking is very efficient for improving the range precision for the LRM data, we did not apply the two-pass retracking for the CryoSat-2 SAR- and SARin-mode data as there is no gain in range precision from the second step of the retracking for SAR and SARin data. This was first documented by Garcia et al., (2014).

2.1.2. 2-Hz Sea Surface height data

The 20/40Hz double retracked SSH data are edited for outliers and subsequently, an along-track low-pass filter is applied before generating the 2Hz SSH data used for the subsequent MSS determination.

The along-track low pass filter uses the Parks-McClellan algorithm which has a cut beginning at 10 km wavelength and zero gain at 5 km, thus the filter has 0.5 gain at 6.7 km, which is approximately the along-track resolution of 1-Hz data (Sandwell and Smith, 2009). The filter had to be designed for each satellite mission to match the 0.5 gain at 6.7 km due to the different along-track sampling rates. After this filter is applied the data were down-sampled to a 2-Hz sampling rate, which corresponds to an along-track spacing of around 3.3 km.

For the previous DTU15MSS, we used 1-Hz SSH data from the Radar Altimetry Data Archive (RADS, Scharroo et al., 2013). In RADS, the 1-Hz data are computed as the average of all 20/40Hz data which is equivalent to using a boxcar filter. The disadvantage of this filer is that spectral leakage in the 10-40 km wavelength which will remain as high-frequency noise in the filtered dataset contributing to the spectral hump of conventional LRM data (Dibarboure et al., 2014; Garcia et al., 2014). The advantage of using the Parks-McClellan algorithm over the boxcar filter is, that this filter has better spectral gain. The filter characteristics are illustrated in Figure 2 for both filters.

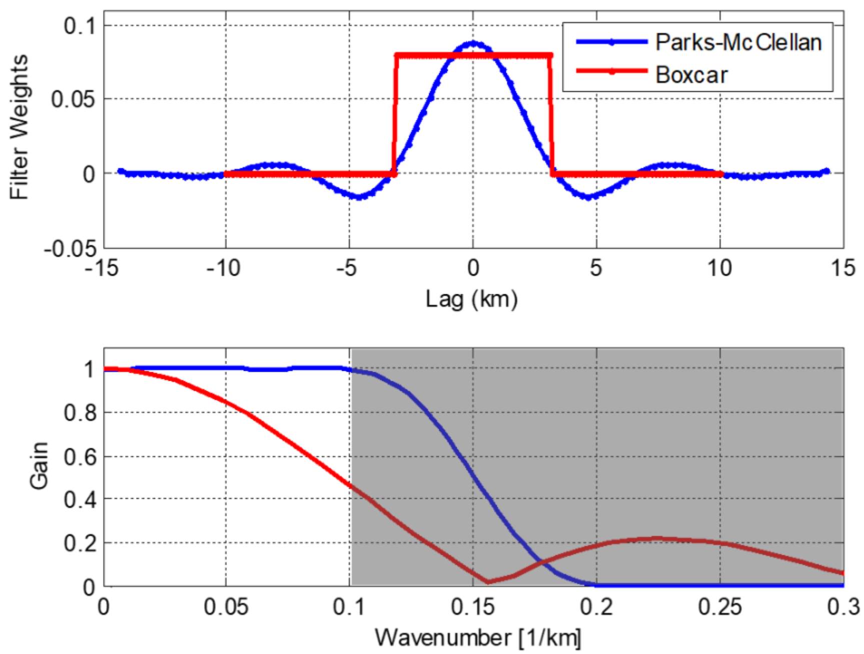

Figure 2: Illustration of Parks-McClellan filter weights (blue) and the boxcar filter (red) to derive 1 or 2-Hz SSH data spatial filter (upper panel). The lower panel illustrates the frequency response of the two filters. Sidelobes and spectral leakage in the 10-40 km wavelength can be seen for the boxcar filter, which will remain as high-frequency noise in the filtered dataset.

2.2 Long wavelength Polar region MSS improvements.

For the polar regions we used the filtered version of DTU15MSS as a prior long wavelength reference. The reason is, that DTU18MSS was based on empirical retracked height in the Polar regions. Frequently, physical and empirical retrackers differ in their height estimation in Polar regions (Rose et al., 2019). DTU15MSS was based on sparse physical retracked data from RADS. However, it was found to be a more consistent prior choice for DTU21MSS where physical retracking is used. Cryosat-2 provides observations all the way to 88N. A closer inspection of the Cryosat-2 mode mask (web1, 2022) shows that Polar Regions (outside the 66 ° parallels) are largely measured in the SAR and SARin modes due to the presence of sea ice. This is with the exception of the Barents Sea north of Norway.

For SAR and SARin mode data we applied the SAMOSA+ physical retracking (Dinardo et al., 2018). SAMOSA+ adapts the SAMOSA retracking model (Ray et al., 2015) to operate over specular scattering surfaces as ice-covered polar oceans by involving mean square slope as an additional parameter in the retracking scheme and by implementing a more sophisticated choice of the fitting initialization resulting in greater robustness to strong off-nadir returns from land or else. The SAMOSA+ retracker even discriminates between return waveforms from diffusive and specular scattering surfaces, ensuring the continuity in the sea level retrieval going from the open ocean and into the leads in the sea-ice.

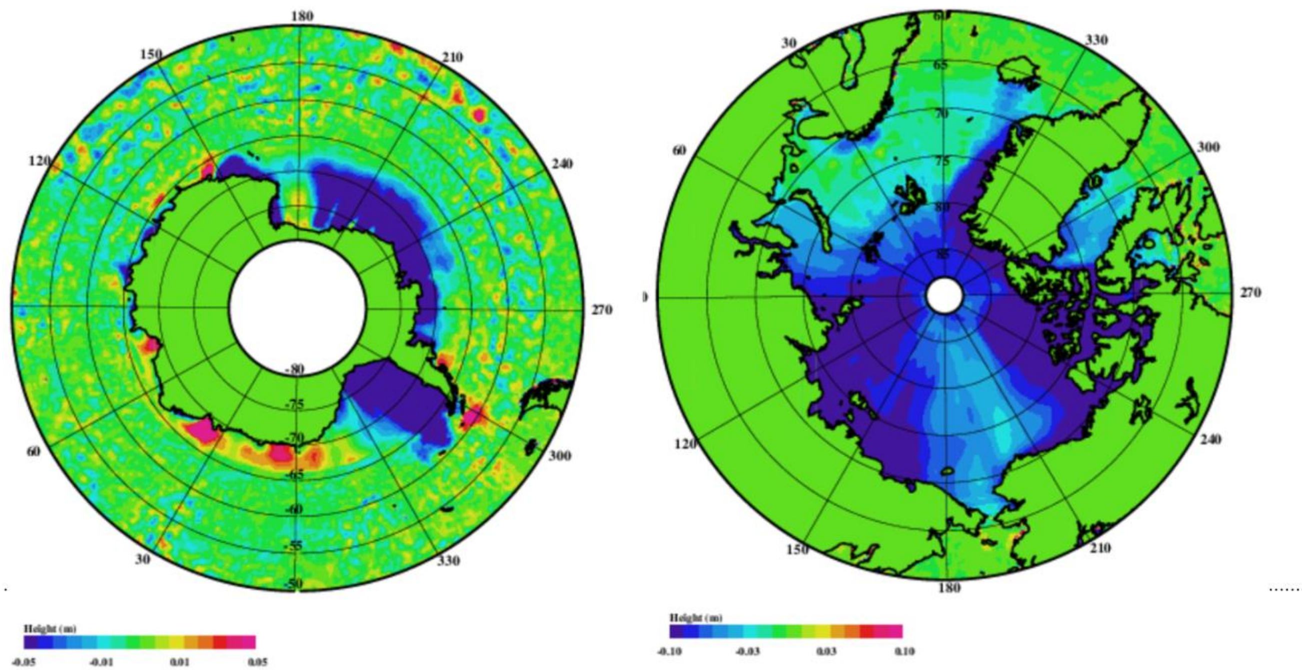

Figure 3. DTU21MSS-DTU15MSS for the Southern Ocean (left) and the Arctic Ocean (right). The color scale ranges up to +/- 5 cm for the Southern Ocean and +/-10cm for the Arctic Ocean.

With the assistance of the European Space Agency (ESA) Grid Processing On-Demand (GPOD) we have processed a total of 9 years of Cryosat-2 (2010.10 to 2019.10) for both the Arctic and the Southern Ocean using this SAMOSA+ retracker. Observations over the sea ice/open ocean interface were removed in the processing and only observations over leads (ocean surface between the ice floes) were selected similar to Rose et al., (2019)

Upon computing the mean profiles of Cryosat-2 observations, the center time for the Cryosat-2 data was 2015.04. It was found that it was necessary to correct for sea level rise to consolidate these data on the 2003.01 center period of the DTU21MSS following the methodology by (Rio and Andersen 2009). This was performed in the 65 ° - 66° border zone as the reprocessing of Cryosat-2 with SAMOSA+ is limited to outside the 65 ° parallels. This resulted in a correction of a few centimeters.

The difference between the DTU21MSS and DTU15MSS is shown in Figure 3 for both the Southern and Polar Oceans. For nearly all ice-covered regions the DTU15MSS is higher than the DTU21MSS. We expect this to be due to the fact that DTU15MSS was derived from 1-Hz RADS data which was very sparse in both time and space. The few data in RADS are a consequence of tight editing and the fact that RADS converts the SAR data to Pseudo LRM (Scharroo et al., 2013) and performed physical retracking on these data using a modified Brown model. In RADS we nearly only found data during the ice-free summer month when the annual signal causes the sea level to stand higher, so it is expected that DTU15MSS could be biased high due to this.

2.3 Mean Sea surface computation

The details of the computation technique of the DTU21MSS follow the development of former DTU MSS models (Andersen and Knudsen, 2008) where the ERM tracks are first used to compute the long wavelength part of the MSS as shown in section 2.2. Hereafter the GM data are introduced to compute the fine-scale structures of the MSS. The fine-scale computation is done in small tiles of 1º x3º with a 0.5 º boundary to parallelize the computation process. As all wavelengths longer than the size of the tiles are removed in this process (roughly 200 km) we found, that there was no need to adjust the period of the GM data to the MSS averaging period (1993-2012).
The final step to close the Polar Gap is to fill in MSS proxy data north of 88N where no altimetry is available. This was done by feathering the EGM08 geoid (Pavlis et al., 2012) across the pole in the following way: The preliminary MSS was calculated up to 88°N using the satellite altimetry data alone. Subsequently, the difference between the MSS and the EGM08 geoid was computed longitude-wise in the 87°N-88°N region and a mean offset was estimated and removed. The residual grid was transformed into a regular grid in Polar stereographic projection enabling interpolation across the North Pole using a second order Gauss Markov covariance function with a correlation length of 400 km. This makes the DTU MSS models truly global.

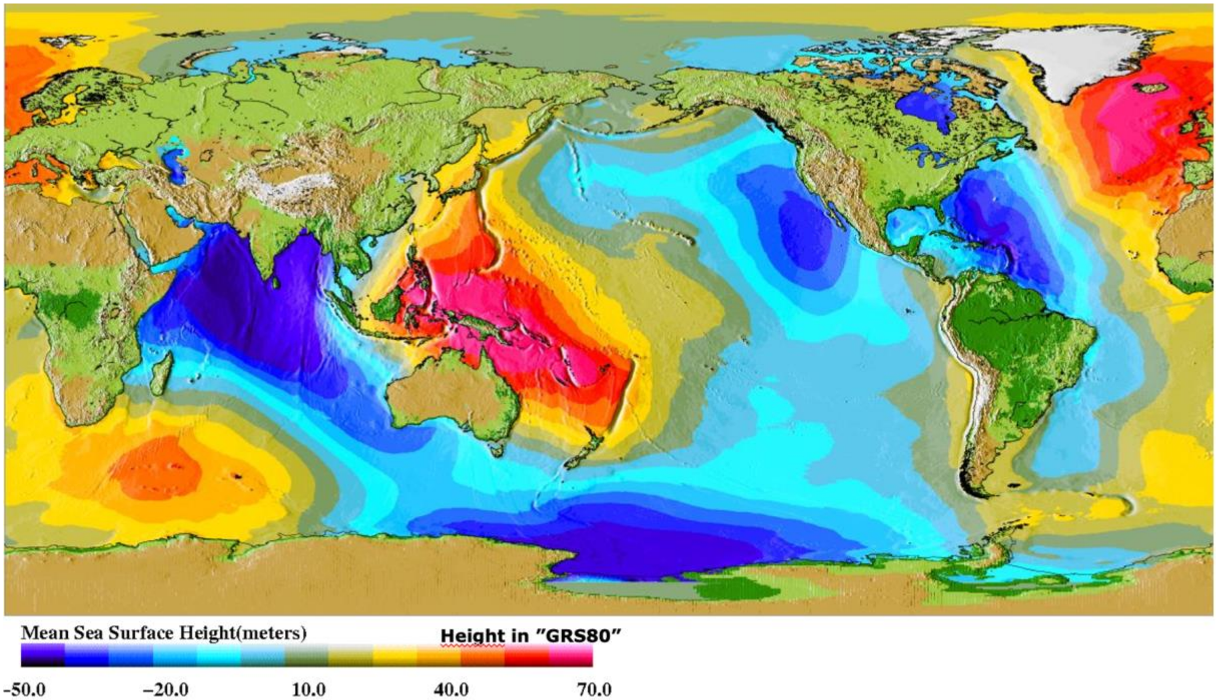

Figure 4: The DTU21 mean sea surface from the Technical University of Denmark (DTU) in meters

The DTU21MSS as its predecessors are all given on a 1-minute global resolution grid. A closer examination of the MSS in Figure 4 illustrates, that the height of the ocean's mean sea surface relative to the mathematical best-fitting rotational symmetric reference system (GRS80) has magnitudes of up to 100 meters.

2.6 Sentinel-3A/B SAR Altimetry

The European Space Agency (ESA) launched Sentinel-3A on the 16th of February 2016 and Sentinel-3B on 25th April 2018. These satellites operate as SAR altimeters everywhere with the benefit of increased range precision compared with conventional LRM altimetry. Both the increased along-track resolution and more importantly the improved cross-track resolution of 35 km for the combined Sentinel 3A/B dataset would make these important contributors to the DTU21MSS. However, two problems prevented the use of these data for the time being.
The first relates to the fact that mean profiles could only be computed over 5 and 3 years from Sentinel 3A and B, respectively. As the Sentinel-3 satellites operate in a 27-days repeat this resulted in as few as 66 and 40 cycles, making these mean profiles considerably noisier compared with other mean profiles. Secondly, the center times of Sentinel 3A/B is 2019 and 2020 which means that the mean profiles are more than 15 years away from the center time of the TOPEX/J1/J2 mean profiles. We illustrate the problem in Figure 5 from a section of the Gulf Stream. The mean of S3A is 8 cm but the standard deviation of the spatial variation with respect to the DTU15MSS is as high as 13 cm (Figure 5 left panel). We show the mean profile from Sentinel-3A along track 719 (located at the blue arrow in the

left panel) across the Gulf Stream going from south to north (right panel of Figure 5). Between 26°N and 32°N the difference corresponds closely to the expected sea level rise of a little more than 8 cm. However, as the track crosses the Gulf Stream the signal increases to nearly 60 cm.
The mean dynamic topography associated with the Gulf Stream causes the mean sea level to drop by around a meter as one moves from the center of the Northwest Atlantic toward the coast. Due to the north/south meandering of the Gulf Stream, it creates the observed sea level residual seen when the averaging period changes (Zlotniki, 1991).
As Sentinel 3A/B are both outside the (1993-2012) averaging period and as the meandering of the Gulf Stream is profound over the last 15 years, it was not possible to ingest the S3A and B mean profiles without degrading the DTU21MSS in this region.
There is no doubt about the importance of Sentinel 3A/B for future MSS models, but to ingest the Sentinel 3A/B in future MSS models we found, that we will need to extend the averaging period to 30 years (1993-2022). We consequently decided only to use the Sentinel 3A/B for the evaluation of the various MSS models.

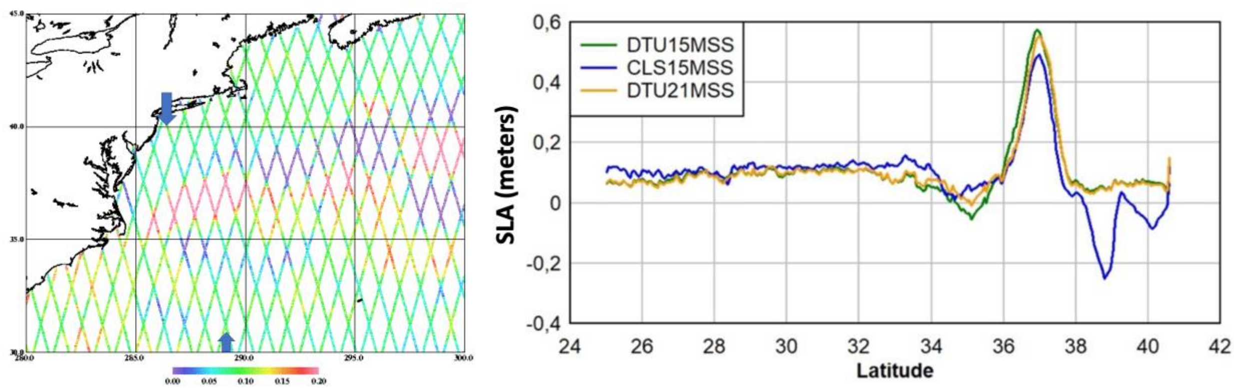

Figure 5: Sentinel-3A 5y mean sea level anomaly along track 791 in the Gulf Stream area relative to DTU15MSS (left). The Sentinel-3A track 791 is located between the with blue arrows in the left figure. The S3A mean anomalies relative to to DTU15MSS, CLS15MSS and DTU21MSS (right).

3. Evaluation

In this section, we perform three different evaluations of the MSS. These evaluations supplement the global evaluation of previous MSS models performed by Pujol et al. (2017) and serve the purpose of indicating the improvements going from DTU15MSS to DTU21MSS globally, in the Arctic Ocean, and in coastal regions. The CLS15MSS is an improvement of the CLS11MSS (Schaeffer et al,, 2012) and is given on a similar 1/60° resolution with a similar averaging period to the DTU MSS models (Pujol et al., 2017). Hence the various MSS models can be directly compared.

3.1 Global evaluation with mean profiles

In the global evaluation, we used data from the 1-Hz RADS data archive. The global comparison in Table 2 illustrates the mean difference and the spatial variation when the mean profiles are spline interpolated onto the various MSS models. The zero offset and small standard deviation for the TP/J1/J2 mean profile are because all MSS are fitted to this profile in its derivation. The small offset for the other mean profiles corresponds to the fact, that the averaging of these profiles is not centered directly at 2003.01. The increased spatial standard deviation for other mean tracks is a consequence of fewer repeat cycles available for these missions. Less than 200 cycles versus 1000 repeat cycles for the TP/J1/J2 mean profiles.

	TP/J1/J2 (541936)	**TP+J1 Interleaved (542638)**	**E2/ENV (1652043)**	**S3A (1446733)**	**S3B (1418477)**
DTU15MSS	0.00 /1.48	0.38 / 3.25	-0.17 / 3.97	4.92 / 5.20	4.94 / 5.39
DTU21MSS	0.00 / 1.17	0.36 / 3.21	-0.14 / 3.40	5.22 / 4.79	5.12 / 5.02
CLS15MSS	0.00 / 1.19	0.32 / 3.11	-0.17 / 5.22	5.26 / 5.01	5.01 / 5.18

Table 2: Comparison with mean profiles given as mean difference and standard deviation of spatial variations. All values are in cm.

The Sentinel 3A and 3B mean profiles are independent of existing MSS models but only 66 and 40 cycles have been used, respectively. In the comparison with the Sentinal-3A/B mean profiles, we limited the comparison to within the 65º parallels. For all comparisons, the number of repeat cycles can be seen through increased standard deviation with decreasing number of repeat cycles. This illustrates the effect of natural variability of the sea surface and how this is gradually averaged out with an increasing number of repeats. The roughly 5 cm mean difference between S3A/B mean profiles and the MSS models directly illustrates the effect of global sea level rise during the altimetric era. 5 cm roughly corresponds to the well-known 3 mm/year sea level rise accumulated between the center period of 2003.01 for the MSS and the averaging period of S3A/B some 15 years later. All comparisons indicate that the DTU21MSS performs slightly superior compared with all older models.

3.2 Arctic Evaluation.

Within the ESA CryoTempo project, we evaluated the impact of the use of a physical retracker and an empirical retracker on the retrieval of sea level anomalies in the Polar Ocean. We used the state-of-the-art empirical retracker called the Threshold First Maximum Retracker Algorithm (TFMRA) (Helm et al., 2014) and the SAMOSA+ physical retracker. In the evaluation, we also compared the state-of-the-art MSS models which were the DTU15MSS and DTU21MSS. It was not possible to include the CLS15MSS as this model only covers up to 84ºN and has several voids in the Arctic Ocean (Pujol et al,, 2017). The use of the physical retracker allows us to estimate the Sea State Bias (SSB) which was estimated. This Sea State Bias correction was subsequently applied to both the SAMOAS+ physical SLA and the empirical TFMRA SLA.

A total of 7 months of Cryosat-2 was used between Oct 3013 and April 2014. The results are shown in Figure 6 where the Upper panels show the spatial variation in the mean (two left panels for the TFMRA and SAMOSA+ retracked SLA) and the corresponding standard deviation of SLA (two right panels). The lower panels highlight the time evolution of the monthly SLA anomalies averaged with the monthly mean given in the left panel and the standard deviation given in the right panel.

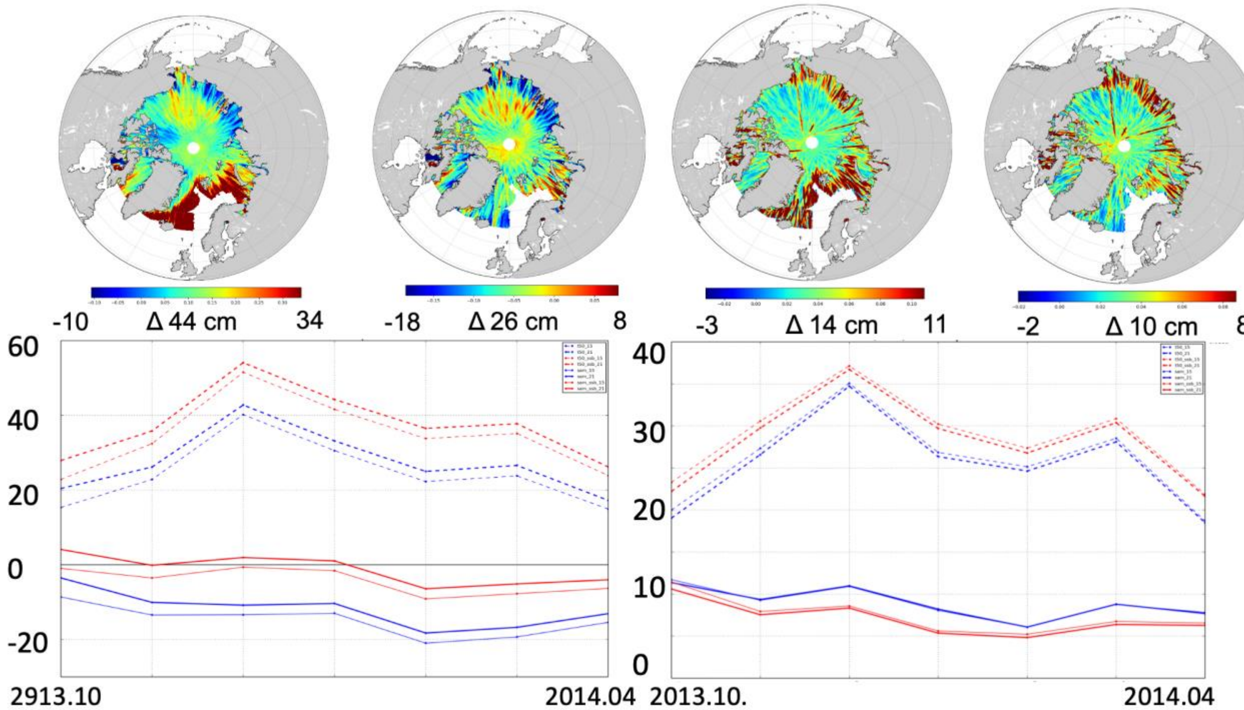

Figure 6. Comparison of retrackers and MSS models over the Arctic Ocean from Oct 3013-April 2014. Upper panels: Mean SLA using the empirical TMFRA retracker and DTU15MSS (first panel); Mean SLA using SAMOSA+ and DTU21MSS (second panel). The standard deviation of SLA using the empirical TMFRA retracker and DTU15MSS (third panel) and standard deviation of SLA using SAMOSA+ and DTU21MSS (fourth panel).
Lower panels: Evolution of SLA in time. The mean (left) and Standard deviation (right) are shown as monthly values. Heavy lines correspond to using DTU21 and thin lines correspond to using DTU15. The dotted lines correspond to using the TFMRA retracker and the solid lines to the SAMOSA+ retracker. The red lines have the Sea State Bias correction applied whereas the blue lines have not.

This study shows an improved measurement of SLA using the physical SAMOSA+ retracker and in all cases, the DTU21MSS delivers better results than the DTU15 MSS. When using the physical SAMOSA+ retracker er can see, that there is a clear effect of the ability to determine and correct for the sea state bias (SSB). With SAMOSA+ sea state bias applied referenced to DTU21MSS we obtain a mean SLA of -1.5cm ±12cm instead of -5.4cm±22cm over the 2013/10-2014/04 period when using an empirical retracker and DTU15MSS

To illustrate the difference between various MSS models across the Arctic Ocean, we computed the difference between the DTU21MSS and the DTU15MSS and CLS15MSS, respectively.

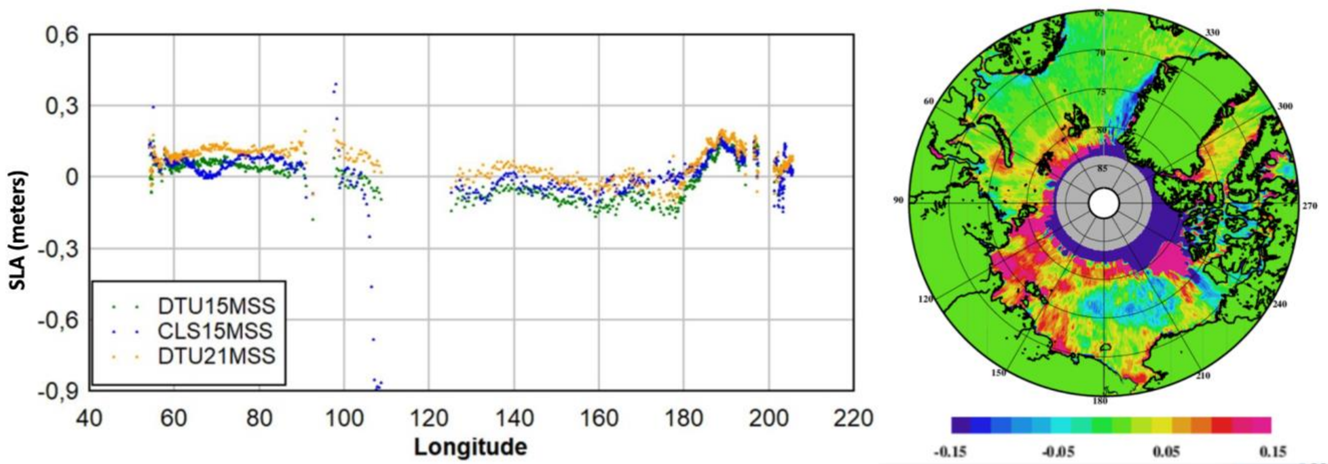

Figure 7. Sea level anomalies (in meters) between the 5-year S3A mean profile along track 497/498 and various MSS models in the Arctic Ocean (left). Right: Mean Sea Surface difference between DTU21MSS and CLS15MSS Dark Blue Regions north of Canada are voids in the CLS15MSS. The color scale ranges from -15cm to +15 cm.

To illustrate the differences between the various MSS model we computed the difference with a Sentinel-3A 5-year mean profile and the various MSS model. Figure 7 shows this difference along the Sentinel-3A track 497/498. The track transits from Russia at 68ºN, 54ºE. Passing to the east of Nova Zemlya and continues up to 82ºN (at 120ºE). From here it descends towards the Aleutian Trench at 57ºN, 204ºE. The standard deviation with the S3A mean profiles are 6.1 5.7 and 8.1 cm respectively for the DTU15MSS, DTU21MSS, and the CLS15MSS. The missing data around latitude 90ºE is due to the crossing of the Russian island Komsomoles. The missing data around 120ºE are due to voids in CLS15MSS causing the S3A data to be removed by the space agencies. The color scale ranges from -15cm to +15 cm. The increase in the S3A residuals around 190°E is associated with the transition of the Bering Strait and the in/out flow through the Strait (Woodgate and Peralta-Ferriz, 2021)

3.3 Coastal evaluation

The difference between the DTU21MSS and the DTU15MSS was evaluated in the Baltic Sea as part of the BalticSeal+ project (http://balticseal.eu/). Differences are presented in Figure 8 (left) panels and are ranging up to 8 cm in the coastal zone and inside the narrow Danish Straits as well as the Bay of Botnia and the Swedish archipelago. In all locations we found, that the former DTU15MSS is unreasonably high near the coastline. Around the coast of Denmark, we further compared with the vertical reference frame model of Denmark called DVR90 (Web2, 2023). DVR90 is fitted to 14 GNSS stations along the coastline of Denmark. The right panel shows illustrate that DTU21MSS has a lower standard deviation close to the coast compared with DTU15MSS which independently verifies that DTU21MSS is superior in fitting Mean Sea Level close to the coast.

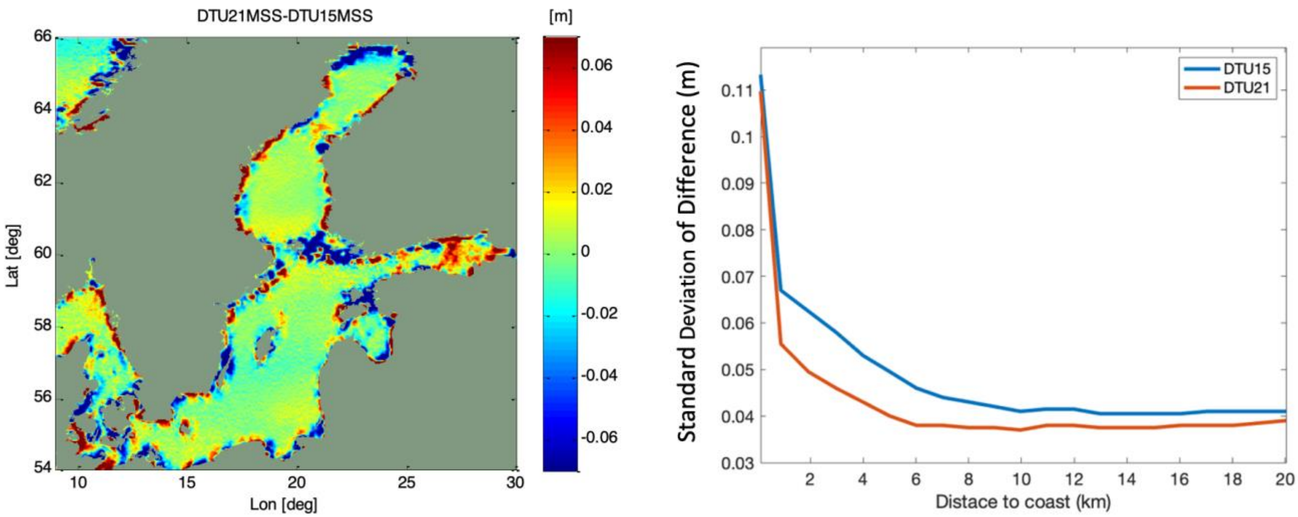

Figure 8: Difference between the DTU21MSS and the DTU15MSS in the Baltic Sea (left). Standard deviation (meters) relative to the the Danish Vertical reference model DVR90 as a function of distance to coast (right).

4. Conclusions

A new Mean Sea Surface (MSS) called DTU21MSS for referencing sea level anomalies from satellite altimetry has been presented along with the first evaluations. We have presented the updated processing chain with updated editing and data filtering. The updated processing filters the double retracked 20-Hz sea surface height data using the Parks-McClellan filter to derive 2-Hz sea surface anomaly. This Parks-McClellan filter has a clear advantage over the 1 Hz boxcar filter used for older DTU models in enhancing the MSS in the 10-40 km wavelength band. Similarly, the use of the FES2014 ocean tide model improves the usage of sun-synchronous satellites in high latitudes in the new MSS.
Cryosat-2 employs SAR and SARin modes in a large part of the Arctic Ocean due to the presence of sea ice. For SAR and SARin mode data we applied the SAMOSA+ physical retracking (Dinardo et al., 2018) to make it compatible with the physical retracker used for conventional Low-Resolution Mode data in other parts of the global ocean.
We initially performed global comparisons with the mean profile from various available satellites using data from the RADS data archive as these have only been used in the DTU15MSS and not any of the other MSS models. The comparison with the independent 5- and 3-year S3A and S3B mean profiles show a relatively clear improvement for the DTU21MSS. This was also expected as the S3A/B satellites employs SAR altimetry and hence should compare better with the MSS derived using the two-pass altimetry due to the enhanced modeling of the 10-30 km wavelength (Garcia et al., 2013).
The evaluation in the Arctic Ocean indicates an improved measurement of SLA using SAMOSA+ with the DTU21MSS. In conjunction with this physical retracker, the correction of the sea state bias (SSB)

further improves the results. In all evaluations, the DTU21MSS delivers better results than the DTU15 MSS. With SAMOSA+, SSB, and DTU21MSS we obtain a mean SLA of -1.5cm ±12cm instead of -5.4cm±22cm over the 2013/10-2014/04 period.
Coastal evaluation of the new DTU21MSS was performed in the Baltic Sea. The evaluation in the Baltic Sea confirms that DTU15MSS is frequently several cm too high in the coastal zone. This was further demonstrated in an evaluation with the Danish Vertical Reference model based on GNSS observations where DTU21MSS showed superior comparison close to the coast.
For the DTU21MSS we found that the 5-year Sentinel-3A mean profiles (2016.05-2020.05) were too problematic to consolidate onto the 1993-2012 averaging period without degrading the MSS model, particularly in large current regions. Consequently we omitted these data in the DTU21MSS, but also found that we shorth need to extend the averaging period to 30 years soon to enable the use of the important new Sentinel-3A/B data in the next-generation MSS models.

Author Contributions

OA wrote the manuscript and performed the computation of the DTU21MSS. ZS performed the two-pass retracking of all 20/40 Hz Geodetic Mission data. AA developing the software for producing 2 HZ and performed the MSS computations in coastal regions. SKR performed the data processing for SAR and SARin data for the Polar Regions. SF contributed to the MSS validation in the Arctic Ocean.

Funding

ESA contributed to the MSS development through the Baltic+Seal project and the CryoTempo projects. SZ worked at DTU during 2020 supported by the National Nature Science Foundation of China, Grant No. 41804002, by the State Scholarship Fund of China Scholarship Council, Grant No. 201906085024, by Fundamental Research Funds for the Central Universities.

Acknowledgments

The authors are thankful to the space agencies for considering the Geodetic or Long-repeat missions as part of mission operations and for providing these high-quality data to the users. We would like to acknowledge ESA-RSS (Research and Service Support), and in particular B. Abis and G. Sabatino, for their assistance in processing the data with G-POD (http://gpod.eo.esa.int/). We acknowledge the support of ESA to the CryoTempo and Baltic Seal+ project through the contracts: AO/1-10244/20/I-NS & 4000126590/19/I-BG

Data availability statement

The DTU21MSS is available from http://data.dtu.dk. The high-resolution MSS model is available in several formats and relative to various reference ellipsoids (TOPEX and WGS84/GRS80) DOI: https://doi.org/10.11583/DTU.19383221.v1

References

Andersen, O. B.: DTU21 Mean Sea Surface. Technical University of Denmark. Dataset. https://doi.org/10.11583/DTU.19383221.v1, 2022.

Andersen, O.B., Zhang, S., Sandwell, D.T., Dibarboure, G., Smith, W.H.F. and Abulaitijiang, A.: The Unique Role of the Jason Geodetic Missions for High-Resolution Gravity Field and Mean Sea Surface Modelling. Rem. Sens., 13, 646. https://doi.org/10.3390/rs13040646, 2021.

Andersen O.B. and Knudsen P.: Global marine gravity field from the ERS-1 and Geosat geodetic mission altimetry. J. Geophys. Res. 103:8129–8137, 1998.

Andersen O. B. and Knudsen P.: The DTU17 global marine gravity field: first validation results. In: International Association of geodesy symposia, Berlin, Heidelberg. https://doi.org/10.1007/1345_2019_65, 2019.

Andersen O. B. and Scharroo R.: Range and geophysical corrections in coastal regions: and implications for mean sea surface determination. In: Vignudelli S, Kostianoy A, Cipollini P, Benveniste J (eds) Coastal altimetry. Springer, Berlin, pp 103–146, 2011.

Andersen O. B., Knudsen P. and Berry P. A. M.: The DNSC08GRA global marine gravity field from double retracked satellite altimetry. J. Geod. 84(3):191–199, 2010.

Andersen O. B., Knudsen P., Kenyon S. and Holmes S.: Global and Arctic marine gravity field from recent satellite altimetry (DTU13). In: Proceedings 76th EAGE, Amsterdam RAI, the Netherlands. http://doi.org/https://doi.org/ 10.3997/2214-4609.20140897,2014.

Brown, G.: The average impulse response of a rough surface and its applications, IEEE J. of Oceanic Engineering, 2(1), 67–74, 1977.

Dibarboure, G., Boy, F., Desjonqueres, J. D., Labroue, S., Lasne, Y., Picot, N., et al.: Investigating short-wavelength correlated errors on low-resolution mode altimetry. J. of Atm. and Oceanic Tech., 31, 1337–1362. https://doi.org/10.1175/JTECH-D-13-00081.1, 2014.

Dinardo S., Fenoglio, L., Buchhaupt C., Becker M., Scharroo R., Fernandes M. J, and Benveniste, J.: Coastal SAR and PLRM altimetry in German Bight and West Baltic Sea. Adv. in Space Research. 62. http://doi.org/10.1016/j.asr.2017.12.018, 2018

Dufau, C., Orstynowicz, M., Dibarboure, G., Morrow, R. and La Traon, P.-Y.: Mesoscale resolution capability of altimetry: Present and future. J. of Geophys. Res., 121, 4910–4927. https://doi.org/10.1002/2015JC010904, 2016.

Fu L-L. and Cazenave A.: Satellite altimetry and earth sciences: a handbook of techniques and applications. Academic, San Diego, United States, 2001.
Garcia, E., S., Sandwell, D. T. and Smith W. H. F.: Retracking CryoSat-2, Envisat and Jason-1 radar altimetry waveforms for improved gravity field recovery, Geophys. J. Int., Vol 196(3), pp 1402–1422, https://doi.org/10.1093/gji/ggt469, 2014.
Gommenginger, C. et al.: Retracking Altimeter Waveforms Near the Coasts. In: Vignudelli, S., Kostianoy, A., Cipollini, P., Benveniste, J. (eds) Coastal Altimetry. Springer, Berlin, Heidelberg. https://doi.org/10.1007/978-3-642-12796-0_4, 2011.
Helm, V., Humbert A. and Miller, H.: Elevation and elevation change of Greenland and Antarctica derived from Cryosat-2, The Cryosphere, 8 (2014), pp. 1539-1559, 2014.
Lyard, F. H., Allain, D. J., Cancet, M., Carrère, L., and Picot, N.: FES2014 global ocean tide atlas: design and performance, Ocean Sci., 17, 615–649, https://doi.org/10.5194/os-17-615-2021, 2021
Maus, S., Green, C. M., and Fairhead, J. D.: Improved ocean-geoid resolution from retracked ERS-1 satellite altimeter waveforms. Geophys. J. Int., 13, 134(1), pp.243-253, 1998.
Pavlis N. K., Holmes S. A., Kenyon S. C. and Factor J. K.: The development and evaluation of the earth gravitational model 2008 (EGM2008). J Geophys Res V117:B04406. https://doi.org/10.1029/2011JB008916, 2012.
Pujol, M.-I., Schaeffer, P., Faugere, Y., Raynal, M., Dibarboure, G., and Picor, N.: Gauging the improvement of recent mean sea surface models: A new approach for identifying and quantifying their errors, J. Geophys Res Oceans, 123, 5889-5911, https://doi.org/10.1029/2017JC013503, 2017.
Raney, R. K.: CryoSat-2 SAR mode looks revisited. IEEE Geosci Remote Sensing Lett., 9(3), pp.393–397, 2011.
Ray, C., Martin-Puig, C., Clarizia, M. P., Runi, G., Dinardo S., Gommenginger, C. and Benveniste, J.: SAR altimeter backscattered waveform model, IEEE Trans. on Geosci. and Rem. Sens., 53(2), 911–919, 2015.
Rio, M.-H. and Andersen, O. B.: GUT WP8100 Standards and recommended models, ESA GOCE User toolbox, https://earth.esa.int/eogateway/tools/goce-user-toolbox/gut-project-overview, 2009.
Rose, S. K., Andersen, O. B., Passaro, M., Ludwigsen, C. A., Schwatke, C.: Arctic Ocean Sea Level Record from the Complete Radar Altimetry Era. 1991–2018. Rem. Sens., 11, 1672. https://doi.org/10.3390/rs11141672, 2019.
Schaeffer, P., Faugere, Y., Legeais, J. F., Ollivier, A., Guinle, T. and Picot, N.: The CNES CLS11 global mean sea surface computed from 16 years of satellite altimeter data. Mar. Geod., 35, 3–19, 2012.
Scharroo, R., Leuliette, E. W., Lillibridge, J. L., Byrne, D., Naeije, M. C. and Mitchum G. T.: RADS: Consistent multi-mission products, in Proc. of the Symposium on 20 Years of Progress in Radar Altimetry, Venice, 20-28 September 2012, Eur. Space Agency Spec. Publ., ESA SP-710, p. 4 pp. 2013.
Sandwell, D. T. and Smith, W. H. F.: Retracking ERS-1 altimeter waveforms for optimal gravity field recovery. Geophys. J. Int., 163(1), pp.79-89, 2005.
Sandwell D. T. and Smith W, H. F.: Global marine gravity from retracked Geosat and ERS-1 altimetry: ridge segmentation versus spreading rate. J. Geophys. Res. 114(B1): B01411, 2009.
Sandwell D. T., Garcia E. S., Soofi K., Wessel P., Chandler M. and Smith W. H. F.: Towards 1-mGal accuracy in global marine gravity from Cryosat-2, Envisat and Jason-1. Lead Edge 32:892–898, 2013.

Sandwell D. T., Müller R. D., Smith W. H. F., et al.: New global marine gravity model from CryoSat-2 and Jason-1 reveals buried tectonic structure. Science 346(6205):65–67, 2014.
Sandwell D. T., Harper H., Tozer B., Smith W. H. F.: Gravity field recovery from geodetic altimeter missions. Adv Space Res. Https:// doi.org/10.1016/j.asr.2019.09.011, 2019.
Stammer D., Cazenave A.: Satellite altimetry over oceans and land surfaces. CRC Press, Boca Raton. https://doi.org/10.1201/ 9781315151779, 2017.
Veng, T., Andersen, O. B., (2020), Consolidating sea level acceleration estimates from satellite altimetry, Adv. in space research, https://doi.org/10.1016/j.asr.2020.01.016
Web1: https://earth.esa.int/eogateway/news/cryosat-geographical-mode-mask-4-0-released, accessed July, 2023)
Web2: https://eng.sdfi.dk/products-and-services/geodesy-and-coordinate-systems, accessed July 2023).
Yuan, J., Guo, J., Zhu, C., Li, Z., Liu, X., and Gao, J.: SDUST2020 MSS: a global 1′ × 1′ mean sea surface model determined from multi-satellite altimetry data, Earth Syst. Sci. Data, 15, 155–169, https://doi.org/10.5194/essd-15-155-2023, 2023.
Zhang S. and Sandwell D. T.: Retracking of SARAL/AltiKa radar altimetry waveforms for optimal gravity field recovery. Mar Geodesy 40(1), 40–56, 2017.
Zhang S., Sandwell D.T., Jin T. and Li D.: Inversion of marine gravity anomalies over southeastern China seas from multi-satellite altimeter vertical deflections. J. Appl. Geophys. 137, 128–137, 2017.
Zhang S., Li J., Jin T. and Che D.: Assessment of radar altimetry cor- rection slopes for marine gravity recovery: a case study of Jason-1 GM data. J. Appl. Geophys. 151:90–102, 2018.
Zhang S., Andersen O. B., Kong X., Li H.: Inversion and validation of improved marine gravity field recovery in South China Sea by incorporating HY-2A altimeter waveform data. Remote Sens 12:802, 2020.
Zlotniki, V.: Sea Level differences across the Gulf Stream and Kuroshio extension. J. Phys. Oceanog., 21(4), 599-609, 1991.
Woodgate, R. A, and Peralta-Ferriz, C.: Warming and Freshening of the Pacific Inflow to the Arctic from 1990-2019 implying dramatic shoaling in Pacific Winter Water ventilation of the Arctic water column. Geophys. Res. Lett., April 2021.DOI: 10.1029/2021GL092528, 2021.